Ultrasonics 138 (2024) 107234

Contents lists available at ScienceDirect

Ultrasonics

journal homepage: www.elsevier.com/locate/ultras

Influence of MHz-order acoustic waves on bacterial suspensions

Nicholas S.L. Chew [a], Chien W. Ooi [b], Leslie Y. Yeo [c], Ming K. Tan [a,*]

[a] Department of Mechanical Engineering, School of Engineering, Monash University Malaysia, 47500 Bandar Sunway, Selangor, Malaysia
[b] Department of Chemical Engineering, School of Engineering, Monash University Malaysia, 47500 Bandar Sunway, Selangor, Malaysia
[c] Micro/Nanophysics Research Laboratory, RMIT University, Melbourne, VIC 3001, Australia

ARTICLE INFO

Keywords:
Bacterial inactivation
Surface acoustic wave
Plasma-activated water
Amplitude modulation
Hybrid modulation

ABSTRACT

The development of alternative techniques to efficiently inactivate bacterial suspensions is crucial to prevent transmission of waterborne illness, particularly when commonly used techniques such as heating, filtration, chlorination, or ultraviolet treatment are not practical or feasible. We examine the effect of MHz-order acoustic wave irradiation in the form of surface acoustic waves (SAWs) on Gram-positive (*Escherichia coli*) and Gram-negative (*Brevibacillus borstelensis* and *Staphylococcus aureus*) bacteria suspended in water droplets. A significant increase in the relative bacterial load reduction of colony-forming units (up to 74%) can be achieved by either increasing (1) the excitation power, or, (2) the acoustic treatment duration, which we attributed to the effect of the acoustic radiation force exerted on the bacteria. Consequently, by increasing the maximum pressure amplitude via a hybrid modulation scheme involving a combination of amplitude and pulse-width modulation, we observe that the bacterial inactivation efficiency can be further increased by approximately 14%. By combining this scalable acoustic-based bacterial inactivation platform with plasma-activated water, a 100% reduction in *E. coli* is observed in less than 10 mins, therefore demonstrating the potential of the synergistic effects of MHz-order acoustic irradiation and plasma-activated water as an efficient strategy for water decontamination.

1. Introduction

Ingesting surface water contaminated with sewage, human or animal waste poses a tremendous microbial risk due to it being a carrier of pathogenic microorganisms. This is especially true for coastal oceanic water and fresh water exposed to wastewater discharges that pollute them with fecal microorganisms and pathogens [1,2]. Of the numerous types of bacteria found in contaminated water, common bacteria that cause waterborne diseases include the various pathogenic variants of *Escherichia coli* (*E. coli*), such as *Enteropathogenic E. coli* that causes infant and childhood diarrhea, *Enteroinvasive E. coli* that causes dysentry, *Enterotoxigenic E. coli* that causes travelers diarrhea [3,4], *Enteroaggregative E. coli* that causes watery diarrhea [5], and *Enterohemorrhagic E. coli* that causes bloody diarrhea [6]; *Salmonella enterica* that causes typhoid and paratyphoid [7]; *Vibrio cholerae* that causes cholera [8]; and many others. Due to the overwhelming types of bacteria found in contaminated water, coliform groups such as *E. coli* are often used as an indicator of pathogen presence in water because these bacteria are the predominant microorganisms in human waste, are commonly present in huge numbers, and are relatively easy to identify [9].

Briefly, water disinfection can be grouped into physical or chemical methods. The most common among physical methods is boiling as most microbes that are present in water can be killed when the water temperature is increased to 100 °C. Nevertheless, boiling water at large scale is cost ineffective and energy intensive [10]. Ultraviolet (UV) irradiation is another common method for disinfection. However, this method requires additional disinfectants to combat photo-reactivated microbes [11] and forms low levels of carboxylic acids and aldehydes, which are potentially harmful compounds [12,13]. Additionally, higher intensities in UV irradiation are required to kill viruses—more than ten times that needed to inactivate *Giardia lamblia*, a common diarrhea-causing parasite [14]. Filtration methods, which employ either microfiltration and nanofiltration membranes to separate particles down to 0.1 μm and 1 nm diameter [15], on the other hand, can yield relatively high quality water, but are expensive to maintain and energy demanding. For instance, biofouling, organic and inorganic fouling along with colloidal fouling are the leading cause of deterioration in filtration performance, having a negative impact on operating conditions, cleaning requirements and operating cost [16]. As such, filtration has a short lifespan and is limited by its ability to separate out tinier pathogens, such as viruses.

Chemical microbial disinfection methods, in contrast, are cost effective and commonly employed in large scale water distribution systems.

* Corresponding author.
E-mail address: tan.ming.kwang@monash.edu (M.K. Tan).

https://doi.org/10.1016/j.ultras.2023.107234
Received 18 September 2023; Received in revised form 22 November 2023; Accepted 24 December 2023
Available online 29 December 2023

Chlorine, belonging to the halogen group of elements, is the most widely used chemical disinfectant and has played a central role in effectively eliminating typhoid fever outbreaks and other diseases [17–19]. It can be stored, transported and made readily available for point-of-use applications. However, chlorine produces some potentially hazardous disinfection byproducts that have been shown to be toxic and even carcinogenic [20,21]. Other halogens such as bromine and iodine can also be used for chemical disinfection, but are uncommon and have only been used to treat small quantities of water since they result in increased toxicity levels compared to chlorinated water [22]. A disadvantage of all chemical disinfection using halogens is the odor and off-taste they create.

More recently, plasma-activated water (PAW) has also been shown to be effective for bacteria disinfection [23,24]. Water is said to be plasma-activated after it has been treated with atmospheric pressure plasma [25], leading to the generation of reactive nitrogen and oxygen species, such as nitric oxide [26–28], nitrite and nitrate [29,30], peroxynitrite [31,32], along with hydroxyl radicals [33,34], superoxides [35], ozone [36] and hydrogen peroxide [37]; a few of these reactive species being potent antimicrobial agents [38]. The presence of reactive species can alter the physicochemical properties of PAW, such as decreasing its pH [39,40], and increasing its electrical conductivity [41,42] and oxidation–reduction potential [43,44]. When microbes are exposed to PAW, their cell membrane integrity can be compromised [45,46] as a consequence of excessive oxidative [47] and physical stress in the presence of the reactive oxygen and nitrogen species [48], leading to leakage of potassium, proteins and DNA/RNA from the cell [49]. Moreover, the reactive species can also accumulate in the microbes [50], resulting in degradation and denaturation of its protein and DNA/RNA [51,52]. Common techniques to generate atmospheric pressure plasma are corona discharge [53], plasma jet [54], and dielectric barrier discharge [55].

Ultrasound can also be used to inactivate microbes, by stressing and disturbing the membrane of microbes, either to reduce their viability or increase cellular uptake of antimicrobials [56,57]. More recently, acoustic irradiation at higher MHz-order frequencies (ranging from 10 to 100 MHz) in the form of surface acoustic waves (SAWs) have also been shown to be able to lyse Gram-negative bacteria such as *E. coli* [58], and both red and white blood cells along with the parasitic cell present in blood [59], In the former, the bacterial suspension is exposed to the SAW irradiation as it flows through a microchannel, whereas in the latter, the SAW is coupled into a phononic lattice on a superstrate atop the SAW device to generate an azimuthal microcentrifugal flow through symmetry breaking of the acoustic wave [60,61].

In this study, we examine the coupling of the SAW directly into a sessile droplet containing the bacterial suspension at far lower excitation powers (10^{-3}–10^{-1} W) to the 10^{-1}–10^{2} W employed, for example, in Ref. [58]. The weaker acoustic streaming flow that arises as a consequence of these lower powers is therefore less likely to result in appreciable shear stress on the bacteria. In addition to allowing us to study the direct effect of the acoustic radiation force on bacterial inactivation (Section 3.1), such an approach involves a much simpler setup that eliminates the need for microchannel and pump, and, more importantly, involves a much lower power consumption. Additionally, we demonstrate that the efficiency of bacterial inactivation can be further increased through the combined synergistic effects of both the MHz-order SAW field and PAW (Section 3.2) and also evaluate the impact of four different excitation schemes—(1) constant-amplitude excitation, (2) amplitude modulation [62], (3) pulse-width modulation [58,63], and (4) hybrid modulation involving a combination of both amplitude and pulse-width modulation [64]—on the efficiency of the bacterial inactivation process (Section 3.3). Finally, we demonstrate that the platform can also be used to disinfect Gram-positive bacteria, specifically *Brevibacillus borstelensis* (*B. borstelensis*) and *Staphylococcus aureus* (*S. aureus*), which have significantly thicker cell walls and hence are more difficult to inactivate compared to their Gram-negative counterparts (Section 3.4).

2. Experimental method

The surface acoustic wave (SAW) device used in this study consisted of a 500 μm thick 128° rotated Y-cut X-propagating single-crystal lithium niobate (LN) piezoelectric substrate (Roditi Ltd., London, UK) on which a focusing elliptical single-phase unidirectional transducer (FE-SPUDT) was fabricated (Fig. 1(a)) using standard UV photolithography. To generate the SAW, a sinusoidal electrical signal from a function generator (AFG1062; Tektronix Inc., Beaverton, OR, USA) and amplifier (ZHL-5W-1; Mini-Circuits Inc., New York, USA) was applied to the FE-SPUDT at its resonant frequency $f_{SAW} = 30.5$ MHz, which is determined by the spacing and width of the fingers in the FE-SPUDT.

Besides constant-amplitude excitation of the input signal to the SAW device (Fig. 1(b-i)), we also employed a variety of modulation schemes to reduce the required input power to the device. For amplitude modulation (Fig. 1(b-ii)), the total power of the electric signal to the FE-SPUDT can be calculated as $P_e = P_c(1 + m^2/2)$, where $P_c = V_c I_c$ is the RMS power of the carrier signal and $m = V_m/V_c$ is the modulation index, $V_m = (V_{max} - V_{min})/2$ is the modulated signal voltage and $I_c = (I_{max} + I_{min})/2$ is the carrier signal current [65]. V_{max} and V_{min} are the maximum and minimum RMS voltages, respectively, whereas I_{max} and I_{min} are the maximum and minimum RMS currents, respectively, all of which were measured using an oscilloscope (TDS 2012C; Tektronix Inc., Beaverton, OR, USA) connected with voltage (TPP 0201; Tektronix Inc., Beaverton, Oregon, USA) and current (P6022; Tektronix Inc., Beaverton, OR, USA) probes. The same amplitude modulation parameters were adopted to those in previous studies [66–69]: modulation frequency $f_m = 1$ kHz and modulation index $m = 0.5$. For pulse-width modulation (Fig. 1(b-iii)), we estimated the input electric power by multiplying the total power with the time ratio R_t between the on- and off-cycles over one complete pulse-width modulation period t_{pw}. The time ratio R_t is defined as $N_{on}/(N_{on} + N_{off})$, where N_{on} represents the number of on-cycles and N_{off} represents the number of off-cycles. In this study, number of on- and off-cycles were fixed at $N_{on} = 200$ and $N_{off} = 200$ such that $R_t = 0.5$. In addition, we also examined a hybrid modulation scheme that involved a combination of both amplitude and pulse-width modulation (Fig. 1(b-iv)).

2.1. Production of plasma-activated water

We first crafted a needle array consisting of 10 shortened needles fixed together side-by-side. This was then connected to the positive terminal of a high voltage DC power supply (SRS PS375; FuG Elektronik GmbH, Rosenheim, Germany); a round aluminum plate served as the ground electrode and was connected to the negative terminal of the power supply. To create a stable atmospheric pressure plasma, we placed the aluminum plate in a Petri dish filled with water and positioned the aforementioned needle array above the water surface. This setup enabled the generation of a strong atmospheric pressure plasma directed towards the water under a sufficiently high electric field (≈ 10 kV). We varied the duration of the plasma treatment to achieve different electrical conductivity levels in the PAW (approximately 50, 150, and 250 μS/cm). The conductivity levels were measured using a conductivity meter (Lutron CD-4306; SIL Technology Sdn. Bhd., Subang Jaya, Selangor, Malaysia).

2.2. Quantification physical properties of the mixtures

The electrical conductivity of all solutions/mixtures were measured using a conductivity meter (Lutron CD-4306; Lutron Electronic Enterprise Co. Ltd, Taipei City, Taiwan), while the pH was quantified using pH test strips (pH-Fix 0-14 REF-92110; Macherey-Nagel Gmbh, Düren, Germany). The density and surface tension of the solutions were measured with a force tensiometer (Sigma 702; Dyne Testing Ltd., Lichfield, UK), and the viscosity was measured using a rheometer (MCR 102; Anton Paar, Graz, Austria). For PAW, the concentration

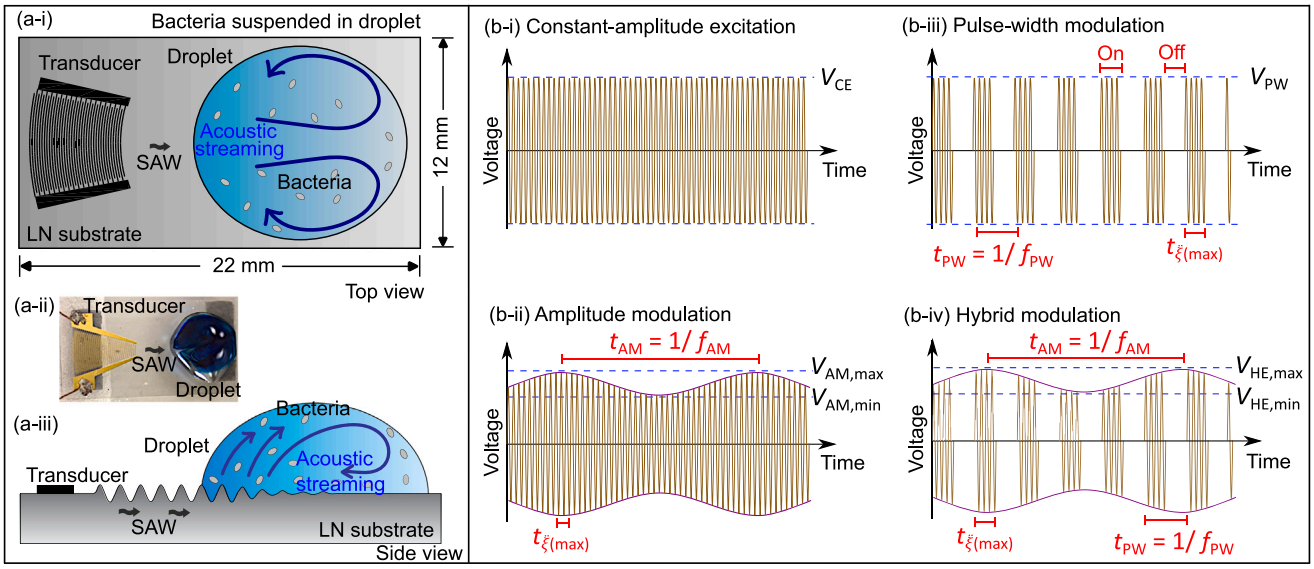

Fig. 1. (a) Experimental setup for studying the effect of SAWs on bacterial suspensions. (a-i, a-ii) top and (a-iii) side view schematics (not to scale) showing a sessile droplet containing the bacterial suspension atop the SAW device (LN substrate on which the FE-SPUDT is patterned; f_{SAW} = 30.5 MHz). The volume of the droplet was 50 μℓ and its diameter (after being dispensed on the LN substrate) was approximately 8 mm. The distance from the transducer to the leading edge of the droplet was approximately 4.5 mm. (b) Four different excitation schemes were examined in this work: (b-i) constant-amplitude excitation, (b-ii) amplitude modulation, (b-iii) pulse-width modulation, and (b-iv) hybrid modulation involving a combination of both amplitude and pulse-width. For constant-amplitude excitation, V_{CE} represents the peak-to-peak voltage. For amplitude modulation, $V_{AM,max} < V_{CE} < V_{AM,min}$; increasing the amplitude modulation index m increases the difference between $V_{AM,max}$ and $V_{AM,min}$. For pulse-width modulation, the maximum peak-to-peak voltage is also higher than that for the constant-amplitude excitation, i.e., $V_{PW} > V_{CE}$. By combining amplitude and pulse-width modulation in the hybrid modulation scheme, the maximum peak-to-peak voltage can be further increased, i.e., $V_{HE,max} > V_{AM,max}$ and $V_{HE,max} > V_{PW}$.

of hydrogen peroxide and nitrate were quantified using dedicated hydrogen peroxide (Quantofix Peroxide 100 REF-91312; Macherey-Nagel Gmbh, Düren, Germany) and nitrate (Quantofix Nitrate 100 REF-91351; Macherey-Nagel Gmbh, Düren, Germany) test strips. To obtain more accurate values, all test strips were read with a test strip reader (Quantofix Relax REF-91346; Macherey-Nagel Gmbh, Düren, Germany).

2.3. Bacterial inactivation

A 50 μℓ droplet of a mixture of the bacteria suspension (both *E. coli* and other Gram-negative bacteria such as *B. borostelensis*) and suspension media solution (either DI water, normal saline (0.9% sodium chloride) or PAW) with a ratio of 1:4 was pipetted onto the SAW device and subsequently subjected to different three different SAW excitation powers ($P_{e=}$ 6, 68 and 348 mW) over 6 different treatment durations (t_{SAW} = 0, 2, 4, 6, 8 and 10 mins).

As the temperature of the SAW device surface increases during treatment and as acoustic streaming is also generated in the droplet, the *E. coli* mixture was separately heat treated and stirred to study the influence of heat and flow on the bacteria in the absence of the acoustic irradiation. In particular, the temperature change on the SAW device at the highest power of P_e = 348 mW at t_{SAW} = 10 mins was first measured with a T-type thermocouple connected to a data logger (GL820, Graphtec Co., California, USA). The *E. coli* suspension was then heat treated and stirred with a hot plate (C-Mag HS7; IKA-WerkeGmbH & Co. KG, Cologne, Germany) stirrer to study the effect of temperature on the bacteria. To investigate the speed of the *E. coli* bacteria in the droplet during the SAW treatment, we emulated the treatment with the same droplet volume and treatment power, but with a normal saline solution containing fluorescent particles with sizes comparable to that of *E. coli* (Fluoresbrite® YG 1.00 μm Microspheres; Polysciences, Inc., Warrington, PA, USA). The droplet containing the fluorescent particles was then placed and observed under the UV light of a microscope (Eclipse Ci-E; Nikon Inc., Tokyo, Japan) with the aid of a high-speed camera (HAS-EF; DITECT Corp., Tokyo, Japan). The speed of the particles were then estimated by using particle tracking software (DiaTrack; Semasopht, Chavannes, Switzerland). The weight of the suspension was quantified using a high precision weighing machine (MS303S; Mettler Toledo, Greifensee, Switzerland).

After the bacterial colonies were exposed to the SAW treatment with various different suspension media solutions, they are plated on their respective type of agar Petri dishes based on the bacteria type and incubated at 37 °C over a duration of 16, 40 and 15 h for *E. coli*, *S. aureus* and *B. borostelensis*, respectively. A relative load reduction of colony-forming units (CFUs) before and after the treatment can then be used to estimate the bacteria inactivation efficiency of the SAW-driven treatment:

$$\eta_e = \frac{CFU_{control} - CFU_{treated}}{CFU_{control}} \times 100\%. \quad (1)$$

2.4. Preparation of bacterial suspensions and bacterial colonies on agar plates

2.4.1. Escherichia coli (E. coli)

A 200 μℓ *E. coli* (BL21 and DE3 strains) suspension was cultured in 10 mℓ of Luria-Bertani (LB) broth, prepared by mixing 0.25 g of LB broth powder (LB Broth Miller 1.10285.0500; Merck KGaA, Darmstadt, Germany) with 10 mℓ of DI water along with 10 μℓ of 25 mg/mℓ kanamycin and 10 μℓ of 30 mg/mℓ chloramphenicol, followed by autoclaving (HICLAVE HV-110; Hirayama Manufacturing Corp., Osaka, Japan) for 15 mins at 121 °C. The cultivation process lasted for 16 h at 37 °C and 200 rpm in an incubation shaker (Certomat® IS; Sartorius Stedim Biotech GmbH, Goettingen, Germany). 1 mℓ of the culture was subsequently added to 50 mℓ of the LB broth along with 50 μℓ of 25 mg/mℓ kanamycin (kanamycin sulfate CAS 25389-94-0; Thermo Fisher Scientific Inc., Waltham, MA, USA) and 30 mg/mℓ chloramphenicol (Calbiochem® Chloramphenicol CAS 56-75-7; Merck KGaA, Darmstadt, Germany), respectively, which was further incubated in the incubation shaker for 5 h at 37 °C and 200 rpm until the optical density (O.D.) of the culture, measured using an absorbance microplate reader (Infinite M Nano; Tecan Group Ltd., Männedorf, Switzerland), increased by 1.0 with a logarithmic growth phase of approximately 10^8 CFU/mℓ. 100 μℓ aliquots from the culture were then centrifuged

Table 1
Electrical conductivity σ_e, density ρ, viscosity μ, surface tension γ, pH, hydrogen peroxide H_2O_2 concentration, and nitrate ion NO_3^- concentration for the various different solutions. Plasma-activated water (PAW) with three different electrical conductivities (σ_e = 0.05, 0.15 and 0.25 mS/cm) were produced using the atmospheric pressure plasma system. Mixture refers to solutions that have been mixed with normal saline (NS) to a ratio of 1:4., i.e., one part normal saline (without bacteria) and four parts of either DI or PAW.

Solution	Abbrev.	σ_e (mS/cm)	ρ (kg/m^3)	μ (mPa s)	γ (mN/m)	pH	H_2O_2 (mg/ℓ)	NO_3^- (mg/ℓ)
Normal saline	NS	12.49	1000.3	0.9936	74.58	7.9	–	–
DI water	DI	–	996.3	0.8997	71.34	7.1	–	–
NS+DI (1:4) mixture	DIM	2.88	997.2	0.9194	73.72	7.4	–	–
Plasma-activated water (Low σ_e)	PAW-L	0.05	996.7	0.9124	71.22	5.3	7	29
NS+PAW-L (1:4) mixture	PAWM-L	2.94	997.9	0.9520	73.66	6.8	3	22
Plasma-activated water (Mid σ_e)	PAW-M	0.15	998.5	0.9283	70.92	4.5	17	76
NS+PAW-M (1:4) mixture	PAWM-M	3.08	999.4	0.9589	73.44	6.4	12	68
Plasma-activated water (High σ_e)	PAM-H	0.25	1001.3	0.9424	70.45	4.0	24	91
NS+PAW-H (1:4) mixture	PAWM-H	3.21	1001.6	0.9740	72.98	5.7	16	83

for 5 mins at 5000 rpm (Sorvall™ Legend™ Micro 21 Microcentrifuge; Thermo Fisher Scientific Inc., Waltham, MA, USA) until a pellet was formed at the bottom of the vial; the remaining liquid slowly removed using a pipette and replaced with 1 mℓ of normal saline (0.9% sodium chloride solution). The vial was subsequently agitated using a vortex shaker (Ika® Genius 3; IKA-Werke GmbH & Co. KG, Baden-Württemberg, Germany) to dissolve the pellet, and the suspension was then serially diluted with normal saline until a concentration of 10^3 CFU/mℓ was achieved.

To prepare the LB agar plates on which the *E. coli* suspension mixture was plated following SAW treatment, 9.25 g of LB agar powder (Miller 1.10283.0500; Merck KGaA, Darmstadt, Germany) was mixed with 250 mℓ DI water and subsequently dissolved through boiling while stirring the mixture. The mixture was then autoclaved for 15 mins at 121 °C and cooled to below 50 °C, following which 250 μℓ of 25 mg/mℓ kanamycin was added. 10 mℓ of this agar mixture was then dispensed into sterile Petri dishes. At least 30 mins was allocated for the agar mixture to set prior to use.

2.4.2. Brevibacillus borstelensis (B. borstelensis)

A 100 μℓ *B. borstelensis* (AK2 strain) suspension was cultured in 10 mℓ nutrient broth (NB) prepared by mixing 0.08 g of NB powder (Miller 105443; Merck KGaA, Darmstadt, Germany) with 10 mℓ of DI water, followed by autoclaving for 15 mins at 121 °C. The cultivation process lasted for 40 h at 37 °C and 150 rpm in the incubation shaker until the O.D. of the culture increased by 0.65. 100 μℓ aliquots from the culture were subsequently centrifuged for 8 min at 5000 rpm until a pellet was formed at the bottom of the vial; the remaining liquid slowly removed using a pipette and replaced with 1 mℓ of normal saline. The vial was then agitated using the vortex shaker to dissolve the pellet, and the suspension serially diluted ten-fold with normal saline.

To prepare the NB agar plates on which the *B. borstelensis* suspension was plated following SAW treatment, 5 g of NB agar powder (Miller 105450; Merck KGaA, Darmstadt, Germany) was mixed with 250 mℓ DI water and subsequently dissolved through boiling while stirring the mixture. The mixture was then autoclaved for 15 mins at 121 °C and cooled to below 50 °C. 10 mℓ of the agar mixture was then dispensed into sterile Petri dishes. At least 30 mins was allocated for the agar mixture to set prior to use.

2.4.3. Staphylococcus aureus (S. aureus)

A 200 μℓ *S. aureus* suspension was cultured in 10 mℓ of Tryptic Soy Broth (TSB) prepared by mixing 0.3 g of TSB broth powder (1224; Condalab S.A., Torrejón de Ardoz, Spain) with 10 mℓ of DI water, followed by autoclaving for 15 mins at 121 °C. The cultivation process lasted for 16 h at 37 °C and 250 rpm in an incubation shaker. After 16 h, 1 mℓ of the culture was added to 50 mℓ of TSB broth and further incubated in the incubation shaker for 4.5 h at 37 °C and 250 rpm until the O.D. of the culture increased by 1.0 with a logarithmic growth phase of approximately 10^{10} CFU/mℓ. 100 μℓ aliquots from the culture were then centrifuged for 7 mins at 5000 rpm until a pellet was formed at the bottom of the vial; the remaining liquid slowly removed using a pipette and replaced with 1 mℓ of normal saline. The vial was subsequently agitated using a vortex shaker to dissolve the pellet, and the suspension was then serially diluted with normal saline until a concentration of 10^3 CFU/mℓ was achieved.

To prepare the TSB agar plates on which the *S. aureus* suspension mixture was plated following SAW treatment, 5 g of TSB agar powder (1224; Condalab S.A., Torrejón de Ardoz, Spain) was mixed with 250 mℓ DI water, and subsequently dissolved through boiling while stirring the mixture. The mixture was then autoclaved for 15 mins at 121 °C and cooled to below 50 °C . 10 mℓ of the agar mixture was then dispensed into sterile Petri dishes. At least 30 mins was allocated for the agar mixture to set prior to use.

2.5. Alternative method for quantifying bacterial inactivation in the suspension

Lamb wave devices similar to that previously reported in the literature [70] were fabricated from the same 500 μm thick LN substrates as the SAW devices. However, instead of patterning the IDTs on the LN, the electrodes simply comprised 10 nm and 200 nm thick layers of titanium and gold uniformly deposited over the entire top and bottom surfaces of the substrate. We note that the surface acoustic wave device is not suitable for the detection in this case since there would be an excessive amount of acoustic energy transmitted into the liquid. The Lamb wave device was partially immersed in the bacterial suspension perpendicularly approximately 0.4 mm above the SAW device, and the insertion loss associated with the transmission of the signal to the device (i.e., the reflection coefficient S_{11} was measured using a vector network analyzer (TR1300/1; Copper Mountain Technologies LLC, Indianapolis, IN, USA) over the frequency range between 1 and 10 MHz (360 scan points). To verify that the change in the S_{11} measurements were correlated with changes in the electrical conductivity of the suspension, we conducted a separate set of measurements in saline solutions with different salt concentrations, in which latex microparticles (Fluoresbrite® Plain YG 1.0 Micron Microspheres; Polysciences Inc., Warrington, PA, USA) of different concentrations were suspended to mimic the bacteria. Briefly, 0.09, 0.135 and 0.18 g of sodium chloride was dissolved in 10 mℓ of deionized (DI) water to obtain saline solutions with electrical conductivities σ_e = 12.5, 16.4 and 21.6 mS/cm, respectively, as measured using the conductivity meter (Lutron CD-4306; SIL Technology Sdn. Bhd., Subang Jaya, Selangor, Malaysia). The concentration of the microparticle suspension, on the other hand, was varied by mixing 1 μℓ of the latex microparticle suspension was initially mixed in the 10 mℓ of DI water, of which 1, 2 and 4 μℓ were further mixed with 2 mℓ of normal saline to obtain particle concentrations of $C_p \approx$ 110, 230 and 450 in a 50 μℓ droplet.

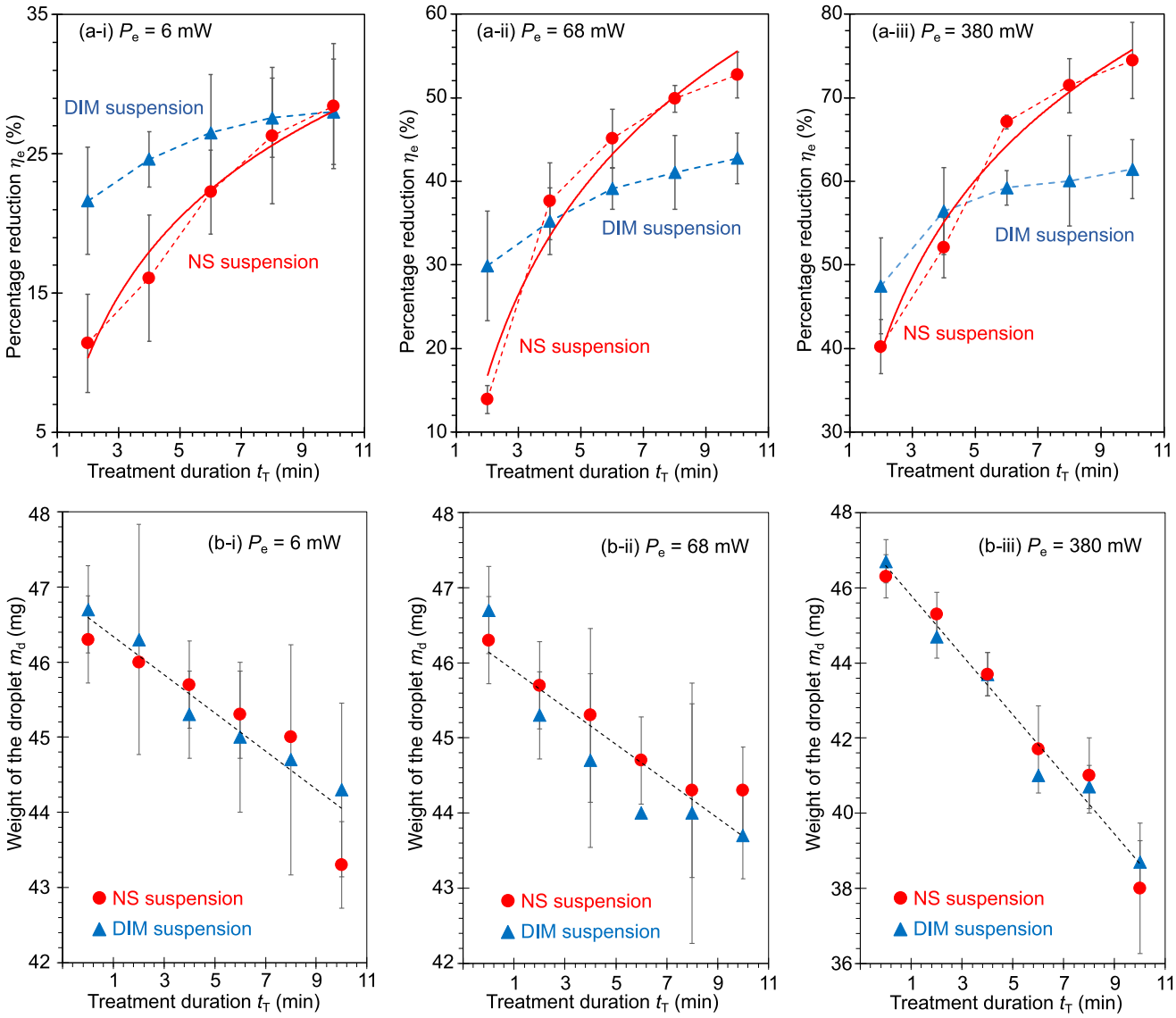

Fig. 2. (a) Relative reduction in bacterial load η_e, and, (b) weight reduction in the droplet m_d, as a function of treatment duration t_T for *E. coli* suspended in a 50 μℓ droplet atop the LN substrate. Three different SAW excitation powers were used: (i) $P_e = 6$ mW, (ii) $P_e = 68$ mW, and, (iii) $P_e = 380$ mW. The *E. coli* was suspended in two different solutions: NS (normal saline) and DIM (mixture of normal saline and DI water); the properties of these two solutions are shown in Table 1. In the calculation of η_e (Eq. (1)), $CFU_{control}$ refers to the NS suspension wherein no SAW treatment was applied ($t_T = 0$). The solid lines represent the fitted curves for the NS suspensions: (a) $\eta_e = 11.01 \ln t_T + 2.72$ ($R^2 = 0.973$), (b) $\eta_e = 24.06 \ln t_T + 0.14$ ($R^2 = 0.962$), and, (c) $\eta_e = 22.51 \ln t_T + 23.9$ ($R^2 = 0.976$). Amplitude modulation with a modulation frequency $f_m = 1$ kHz and modulation index $m = 0.5$ was employed for the SAW excitation in this dataset. Trendlines (dotted lines) were added to aid visualization, and the standard deviation in η_e for each condition was independently calculated from triplicate experiments.

3. Results and discussion

Table 1 presents the measured properties (electrical conductivity σ_e, density ρ, viscosity μ, surface tension γ, pH, hydrogen peroxide H_2O_2 concentration and nitrate ion NO_3^- concentration) of the various solutions used in this study: (1) normal saline (NS); (2) diluted normal saline (DIM); and, mixtures of normal saline with PAW of different electrical conductivities, i.e., (3) PAWM-L (low σ_e), (4) PAWM-M (mid σ_e), and, (5) PAWM-H (high σ_e). NS serves as the control and is used to suspend bacteria prior to the experiments. DIM, with slightly change in physical properties, is employed to compare the effect of the transmitted acoustic waves on bacteria. The three mixtures of normal saline with PAW (PAWM-L, PAWM-M, and PAWM-H) allow us to assess the impact of PAW on the bacterial suspensions. We note that H_2O_2 and NO_3^- were absent in NS, DI water (DI), and the normal saline and DI water mixture (DIM). For the PAW mixtures, there were slight reductions in the H_2O_2 and NO_3^- concentrations after mixing with normal saline. In subsequent experimental studies, only five solutions from Table 1 were utilized: (1) NS, (2) DIM, (3) PAWM-L, (4) PAWM-M, and, (5) PAWM-H.

3.1. Effect of the MHz-order acoustic field on the inactivation of Gram-negative bacteria

Compared to the control, i.e., bacteria suspended in NS solution in the absence of the acoustic treatment ($t_T = 0$), we observe a maximum relative load reduction of $\eta_e \lesssim 74\%$ when the same bacterial suspension is exposed to the SAW at an excitation power of $P_e = 380$ mW, as shown in Figs. 2(a)–2(c). For the same acoustic treatment duration t_T, the relative load reduction can be increased by raising the excitation power. For instance, over short acoustic treatment durations $t_T = 2$ mins, the relative load reduction increases from $\eta_e = 11\%$ to 14% and 40% when the excitation power is increased from $P_e = 6$ mW to 65 mW and 380 mW, respectively. We note that these excitation powers (10^{-3}–10^{-1} W) are still relatively low compared to the typical excitation

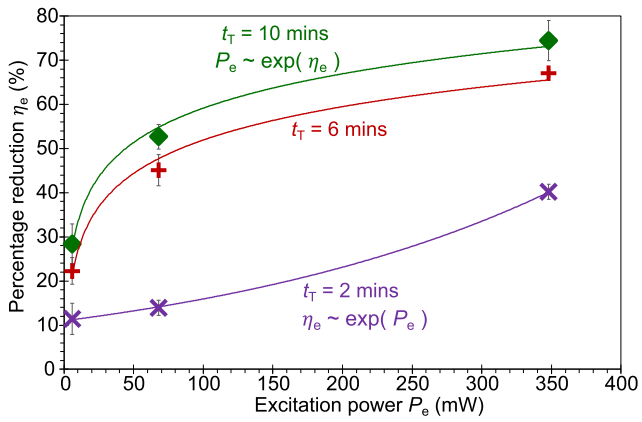

Fig. 3. Replot of the data from Figs. 2(a), 2(b) and 2(c) to show the relationship between the relative load reduction η_e as a function of the excitation power P_e for three different acoustic treatment durations: t_T = 2 mins (×), t_T = 6 mins (+), and t_T = 10 mins (◆). The solid lines represent the fitting of the data: $\eta_e = 10.987\exp(0.004P_e)$ for t_T = 2 mins ($R^2 = 0.999$), $\eta_e = 10.913\ln(P_e) + 1.662$ for t_T = 6 mins ($R^2 = 0.989$), and, $\eta_e = 11.337\ln(P_e) + 7.436$ for t_T = 10 mins ($R^2 = 0.993$). The standard deviation in η_e for each condition was independently calculated from triplicate experiments.

powers required for nebulization under the SAW (> 10^0 W). As can be seen in Fig. 3, the relationship between the relative load reduction and excitation power follows $\eta_e \sim \exp(P_e)$ for t_T = 2 mins. In particular, for shorter acoustic treatment durations, a higher η_e can be achieved with a small increase in P_e. This trend is evident from the observed rise in $\Delta\eta_e/\Delta P_e$ with increasing P_e.

When bacterial suspensions are exposed to the SAW at relatively low powers, for which the acoustic streaming flow that arises as a consequence of the transmission of acoustic energy into the liquid phase is not sufficiently significant to impose appreciable shear stresses on the bacteria, it is likely that the acoustic radiation force imposed on the bacteria plays a central role in their inactivation, particularly given that their diameter ($\phi_{E.coli} \approx$ 0.8–1.0 μm) and length ($L_{E.coli} \approx$ 1.5 – 2.5 μm) [71,72] are considerably smaller than the sound wavelength in the liquid, i.e., $\phi_{E.coli} \ll \lambda_f$ and $L_{E.coli} \ll \lambda_f \approx 49$ μm for $f_{SAW} \approx 30$ MHz. For simplicity, if we assume that the suspended bacteria resembles an elastic spherical sphere submerged in the liquid phase, the acoustic radiation force exerted on it can be approximated by that on a small sphere ($kR_0 \ll 1$) and thus $F_{rad} \sim \dot{\xi}$, where $\dot{\xi}$ being the acoustic particle velocity.[73] Given that increasing the excitation power increases the surface displacement of the LN substrate ($P_e \sim \xi_{LN}$), leading to a subsequent increase in the acoustic particle velocity ($\xi_{LN} \sim \dot{\xi}_{LN}$), it then follows that the acoustic radiation force exerted by the SAW irradiation on the sphere/bacteria is $F_{rad} \sim \dot{\xi}^2 \sim P_e^2$, suggesting a nonlinear relationship between η_e and P_e and hence indicating that the acoustic radiation force has a significant role on bacterial inactivation, at least for the short acoustic treatment durations (t_T = 2 mins) examined.

Despite the acoustic streaming being comparatively weak (from the perspective of shearing and hence disrupting cell membranes) such that the acoustic radiation force assumes the dominant role in inactivating the suspended bacteria, the convective flow associated with the acoustic streaming nevertheless facilitates transport of the bacteria away from the stagnation regions near the droplet contact line where the acoustic radiation force is weak, into the bulk regions of the droplet where the transmitted acoustic waves propagate. The acoustic streaming velocity, which scales as $U \sim \dot{\xi}$, thus increases as the excitation power is increased. At the highest excitation power we use (P_e = 380 mW), the estimated maximum acoustic streaming velocity magnitude is approximately 0.4 mm/s—too low to induce the level of stresses required for shear-driven lysis of the bacteria, but sufficient for their transport. While inducing flow in the bacteria suspension has also been known to enhance bacterial growth by facilitating aeration and nutrient supply as well as removing cell waste, such effects have nevertheless been reported at considerably higher flow intensities. For instance, we only observed appreciable increases in the growth of bacteria colonies on agar plates (approximately 8.2%±4.9% and 25.5%±5.1%) following agitation of bacterial suspensions at velocities of approximately 30 mm/s and 240 mm/s, respectively, with a magnetic stirrer.

Over longer acoustic treatment durations (t_T = 10 mins), we note that the relative reduction in bacterial load increases from η_e = 28% to 53% and 74%, when the excitation power is increased from P_e = 6 mW to 65 mW and 380 mW, respectively. From Fig. 3, we observe that $P_e \sim \exp(\eta_e)$, wherein an exponential increase in excitation power is required to achieve higher relative load reductions—opposite to the trend seen for short acoustic treatment durations (t_T = 2 mins). This is indicated by the decrease in $\Delta\eta_e/\Delta P_e$ as P_e increases. As can be seen in Figs. 2(d)– 2(f), increasing the acoustic treatment duration leads to a more significant reduction in droplet mass due to the slow evaporation that occurs at the liquid–air interface. For example, the reduction in mass at t_T = 10 mins is approximately $\Delta m_d \approx$18% at P_e = 380 mW, whereas Δm_d < 6% for P_e = 6 and 68 mW. The increase in mass loss at higher excitation powers suggests a considerable amount of acoustic energy has been converted to thermal energy, resulting in an increase in the droplet temperature by up to $\Delta T \approx$ 7 °C at P_e = 380 mW, reaching a steady-state value after approximately 3 mins. It is expedient to note, however, that the effect of this level of increase in solution temperature on bacterial inactivation is insignificant compared to the effect of the acoustic field. In fact, a slight increase in the solution temperature can also enhance bacterial growth. For instance, increasing the temperature of the same *E. coli* suspension by 7 °C using a hotplate was seen to lead to an increase in the bacteria colony on the agar plates by approximately 8.7%. As such, it is possible to discount the role of SAW heating on bacterial inactivation.

From Figs. 2(a)–2(c), it can also be seen that the relative reduction in bacterial load increases with longer acoustic treatment durations, scaling as $\eta_e \sim \ln t_T$ for the three different excitation powers. Put another way, the rate of increase in the relative load reduction $\Delta\eta_e/\Delta t_T$ decreases as the acoustic treatment time increases. The physical properties of the solution in which the bacteria are suspended also play a critical factor on the bacteria inactivation. For *E. coli* suspended in diluted saline DIM solutions, the relative load reduction was slightly higher than that for normal saline solution at low excitation powers (P_e = 6 mW) when $t_T \leq$ 6 mins (Fig. 2(a)). In other words, slightly more bacteria were inactivated since DIM solutions do not constitute ideal media to suspend bacteria. However, these differences in relative load reduction become insignificant when t_T > 6 mins. This can be attributed to the stronger acoustic field required to inactivate bacteria suspended in NS solutions. Moreover, the DIM solutions have lower density and surface tension compared to NS solutions (see Table 1), leading to a decrease in efficiency in the transmission of acoustic energy from the LN substrate into the droplet as a consequence of an increase in the difference between the characteristic acoustic impedance of the liquid phase and the LN substrate. Finally, we note that the acoustic radiation force exerted on the bacteria was also seen to be reduced due to lower values of λ_ρ [parenthetically, we note an opposite trend of the SAW irradiation in Refs. [74–76] in which an increase in the digestion of organic matter in wastewater by *E. coli* is reported, rather than inactivation of the bacteria itself; this is likely because clumps/aggregates form when bacteria attach to suspended solids in the wastewater, resulting in their shielding from the potentially disruptive effects of the acoustic pressure wave in that work].

Interestingly, the gradual inactivation of the bacteria with the SAW treatment manifests in a change in the electrical conductivity of the suspension, which can be sensitively captured through changes in the insertion loss S_{11} in the acoustic transmission along a second LN device (that also generates MHz-order acoustic waves but in the form of Lamb waves—see Section 2.5) immersed into the suspension perpendicular

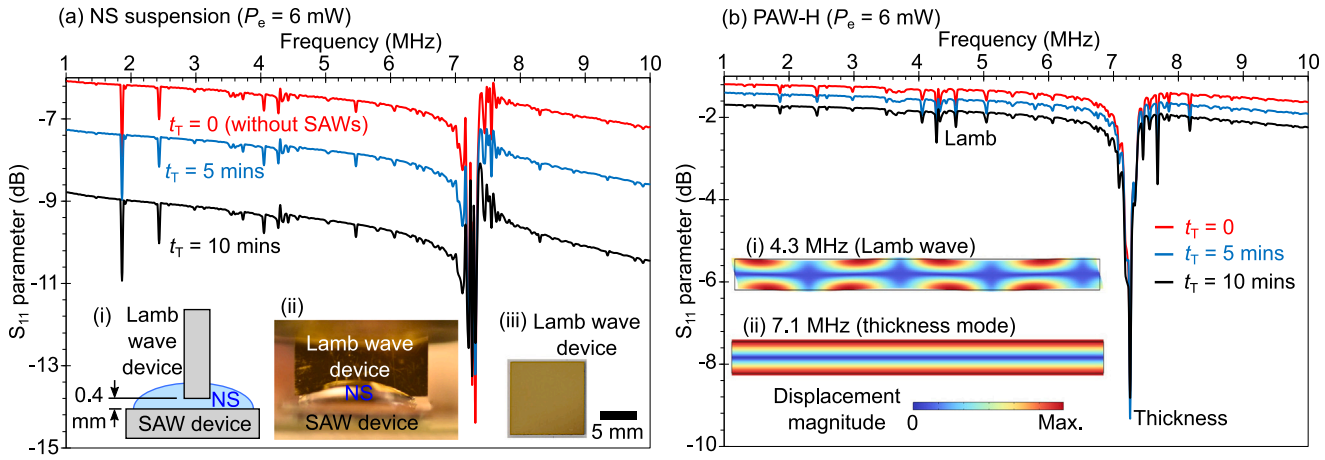

Fig. 4. Insertion loss parameter S_{11} associated with the signal transmission to the Lamb wave device immersed in a 50 μℓ sessile droplet comprising the (a) NS), and, (b) PAW-H *E. coli* samples, perpendicular to the SAW device. The figure insets in (a) show (i,ii) the mounting configuration, and, (iii) the Lamb wave device. The S_{11} measurements were carried out for three different treatment durations: t_T = 0 (control), t_T = 5 mins, and t_T = 10 mins, and the SAW excitation power was fixed at P_e = 6 mW, with the SAW device turned off during the measurements; (following the SAW treatment, the electrical conductivity of the suspension would have increased whereas the number of suspended bacteria would have reduced; the effects arising from these two parameters are presented in Figs. 5(a) and (b), respectively). The resonant frequency observed at approximately 7.3 MHz corresponds to the thickness mode of the Lamb wave device. The insets in (b) illustrate the computed displacement magnitude associated with (i) the Lamb wave and (ii) the thickness mode wave via a simplified numerical model (COMSOL Multiphysics 5.3) in the absence of any liquid loading; in the simulations, the thickness and length of the LN substrate were 500 μm and 6 mm, respectively, whereas gold electrodes of thickness 0.2 μm were placed on the top and bottom surfaces; periodic boundary conditions were applied on the left and right edges of the substrate.

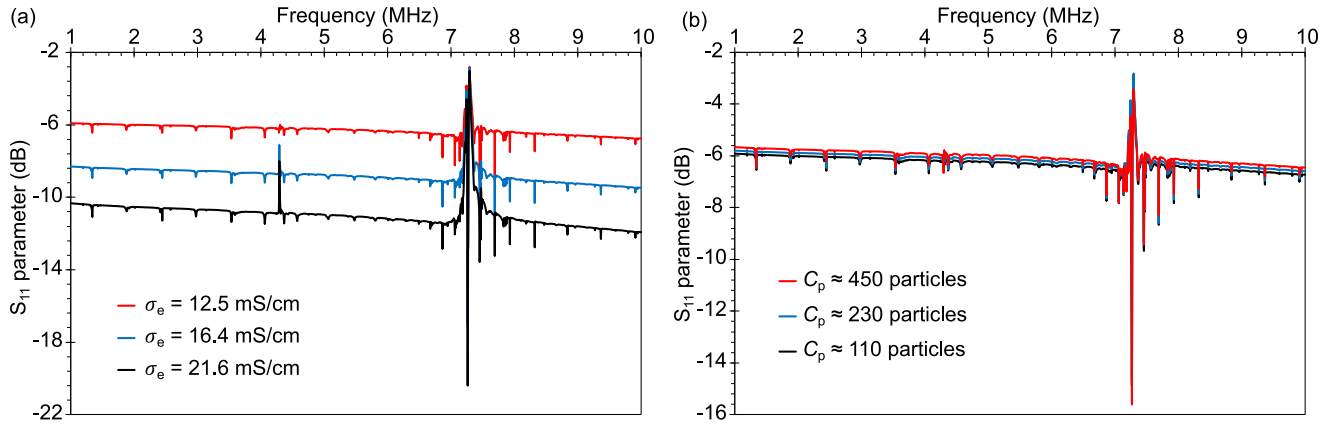

Fig. 5. Insertion loss parameter S_{11} associated with the signal transmission to the Lamb wave device immersed in a 50 μℓ sessile droplet comprising saline solutions with (a) different salt concentrations and hence different electrical conductivities, and, (b) different microparticle concentrations. The setup of the Lamb wave and SAW devices are identical to that shown in the inset in Fig. 4(a-i).

to the SAW LN substrate, as illustrated in the inset of Fig. 4. More specifically, we observe a distinct increase in the overall magnitude of the S_{11} parameter (also known as the reflection coefficient) within the frequency range from 1 to 10 MHz with increasing treatment duration (Fig. 4). A similar shift in the overall magnitude can also be seen with increasing salt concentration of saline solutions suspended with latex microspheres to mimic the bacteria (Fig. 5), therefore alluding to the increasing electrical conductivity as the bacterial suspensions are increasingly inactivated (and to a lesser extent as the number of bacteria in the suspension is reduced)—likely a consequence of the leakage of the cytosol from the bacterial cells as they are lysed. In any case, such a facile method demonstrates the potential for quantifying bacterial activity in a sample without the need for tedious bacteria plating and time-consuming incubation steps.

3.2. Effect of the MHz-order acoustic field and plasma-activated water on the inactivation of Gram-negative bacteria

A significant increase in the relative bacterial load reduction can be further achieved by adding PAW to the suspensions, as shown in Fig. 6. This can be attributed to the presence of H_2O_2 in the PAW, which plays a crucial role in bacteria inactivation. Notably, the PAW mixture with the highest electrical conductivity (PAWM-H, see Table 1) remarkably resulted in effectively deactivating all of the bacteria in the sample completely (η_e = 100%) following treatment at the highest acoustic excitation power (P_e = 380 mW) over a duration of $t_T \geq 8$ mins. The influence of PAW is also evident at lower excitation powers. For instance, at P_e = 6 mW and t_T = 10 mins, the relative load reductions are η_e = 50.2%, 68.3%, and 78.3% for the three PAW mixtures PAWM-L, PAWM-M, and PAWM-H, respectively (Fig. 6(a)). In comparison, under identical excitation conditions (P_e = 6 mW and t_T = 10 mins) with normal saline (NS) solutions, the relative load reduction was only η_e = 28.4% (Fig. 2(a)). This indicates that switching from NS to PAW mixtures can lead to an increase in relative load reduction ranging between $21.8\% \leq \Delta\eta_e \leq 49.9\%$, underscoring the effectiveness of these mixtures for bacterial inactivation. As a side note, without any acoustic treatment (t_T = 0 and P_e = 0), the relative load reductions were η_e = 24.3±4.1%, 28.2 ± 5.5% and 45.3 ± 3.5% for the PAWM-L, PAWM-M, and PAWM-H mixtures, respectively., therefore highlighting the importance of harnessing both the acoustic field as well as the PAW for bacterial inactivation synergistically.

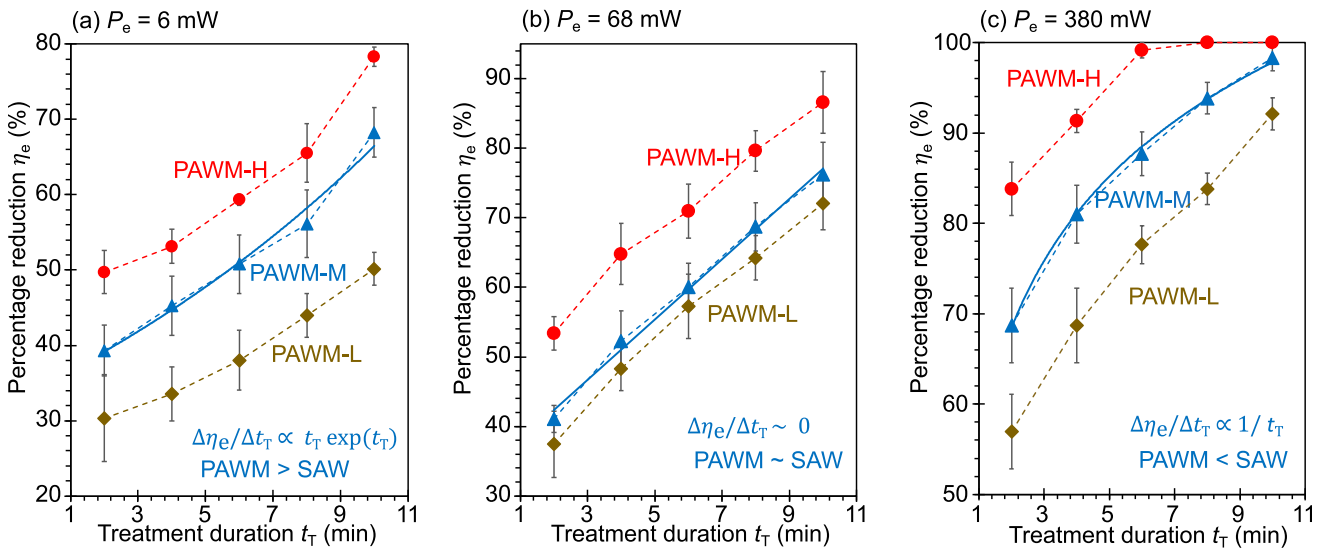

Fig. 6. Relative load reduction η_e as a function of treatment duration (t_T = 2, 4, 6, 8 and 10 mins) for *E. coli* suspensions exposed to the SAW at different powers: (a) P_e = 6 mW, (b) P_e = 68 mW, and (c) P_e = 380 mW. Three different solutions were used: PAWM-L (σ_e = 2.94 mS/cm), PAWM-M (σ_e = 3.08 mS/cm), and PAWM-H (σ_e = 3.21 mS/cm); the properties of these solutions are shown in Table 1. In the calculation of η_e (Eq. (1)) for all suspensions, $CFU_{control}$ refers to *E. coli* suspended in NS solution with t_T = 0. The solid lines for the PAWM-M suspensions represent fitting of the data: (a) $\eta_e = 34.35\exp(0.066t_T)$ (R^2 = 0.984), (b) $\eta_e = 4.34t_T + 33.60$ (R^2 = 0.995), and (c) $\eta_e = 18.27\ln t_T + 55.76$ (R^2 = 0.998). Amplitude modulation with a modulation frequency f_m = 1 kHz and modulation index m = 0.5 was employed for the SAW excitation in this dataset. Trendlines (dotted lines) were added to aid visualization, and the standard deviation in η_e for each condition was independently calculated from triplicate experiments.

Another interesting trend we observed was the changing relationship between η_e and t_T as the excitation power is increased: (1) $\eta_e \sim \exp(t_T)$ at P_e = 6 mW, (2) $\eta_e \sim t_T$ at P_e = 68 mW, and, (3) $\eta_e \sim \ln t_T$ at P_e = 380 mW. The corresponding rate of increase for the relative load reductions is $\Delta\eta_e/\Delta t_T \sim t_T \exp(t_T)$, 0, and $1/t_T$ for the excitation powers P_e = 6 mW, 68 mW and 380 mW, respectively. This suggests that at higher excitation power P_e = 380 mW, the effect of the acoustic field is slightly more dominant, leading to trends similar to those observed for NS solutions (Figs. 2(a)–2(c)), where $\Delta\eta_e/\Delta t_T \sim 1/t_T$. Conversely, at lower excitation power P_e = 6 mW, the effect of PAW is slightly more dominant ($\Delta\eta_e/\Delta t_T \sim t_T \exp(t_T)$). Between these two asymptotic limits at mid excitation powers P_e = 68 mW, both effects appear to contribute appreciably to the bacterial inactivation ($\Delta\eta_e/\Delta t_T \sim 0$), as seen in Figs. 6(a)–6(c).

3.3. Enhancing inactivation of Gram-negative bacteria with a hybrid modulation scheme

We now turn to examine the effect of different excitation schemes on the efficacy of bacteria inactivation. As can be seen in Fig. 7(a), a hybrid modulation scheme that combines both amplitude and pulse-width modulation appears to provide the most significant increase in the relative bacterial load reduction for *E. coli* suspended in various solutions relative to that for constant-amplitude excitation: $\Delta\eta_e$ = 14% in normal saline (NS), $\Delta\eta_e$ = 19% in plasma-activated water mixtures (PAWM-M and PAWM-H); the corresponding statistical significance between the data points are shown in Table 2. This enhancement can be attributed to the higher maximum excitation voltage amplitude achieved with the hybrid modulation scheme. For example, at an excitation power of $P_e \approx$ 68 mW, the maximum peak-to-peak voltages $V_{p-p,max}$ are: $V_{CE,max} \approx$ 4.5 V for constant-amplitude excitation, $V_{AM,max} \approx$ 4.7 V for amplitude modulation, $V_{PW,max} \approx$ 6.1 V for pulse-width modulation, and $V_{HE,max} \approx$ 8.2 V for hybrid modulation, as shown in Figs. 1(b-i)–1(b-iv), respectively. The increase in the excitation peak voltage leads to a greater surface displacement of the LN substrate and, in turn, higher acoustic particle velocities, i.e., $V_{p-p,max} \sim \xi_{LN,max} \sim \dot{\xi}_{LN,max}$. Since the acoustic pressure amplitude increases with increasing acoustic particle velocity $p \sim \dot{\xi}_{LN,max}\rho_0 c$ for a plane acoustic wave, this therefore results in a stronger acoustic radiation force that is exerted on the bacteria.

Table 2
Probability values p from a Student's t-test used to assess the significance (95% confidence interval) of the relative reduction in bacterial load η_e (see Fig. 7(a)) under different excitation schemes (CAE: constant-amplitude excitation, AM: amplitude modulation; PWM: pulse-width modulation, and, HM: hybrid modulation) for *E. coli* suspended in the NS, PAWM-M and PAWM-H solutions. A $p < 0.05$ value denotes a statistically-significant difference in η_e between two data sets.

NS suspension	AM	PWM	HM
CAE	0.127	0.019	0.001
AM	–	0.295	0.018
PWM	–	–	0.041
PAWM-M	**AM**	**PWM**	**HM**
CAE	0.048	0.015	0.001
AM	–	0.240	0.010
PWM	–	–	0.046
PAWM-H	**AM**	**PWM**	**HM**
CAE	0.151	0.013	0.001
AM	–	0.107	0.005
PWM	–	–	0.030

We note that even though the maximum excitation voltage amplitude only occurs over a very short duration over each modulation period (i.e., $t_{\ddot{\xi}(max)} < t_{AM}$ for amplitude modulation, $t_{\ddot{\xi}(max)} < t_{PW}$ for pulse-width modulation, and, $t_{\ddot{\xi}(max)} < t_{PW} < t_{AM}$ for hybrid modulation), this appears to be adequate to inflict sufficient damage on the bacteria to result in their inactivation, as observed by the increase in relative bacterial load reduction with these modulation schemes (Fig. 7(a)).

More specifically, the higher peak-to-peak excitation voltages $V_{p-p,max}$ under modulation schemes can lead to: (1) increased droplet evaporation Δm_d, (2) higher surface temperatures T_{LN}, and, (3) faster streaming velocities U_{dc}. Nevertheless, due to the rather short duration of $V_{p-p,max}$ over one complete modulation period, variations in Δm_d, T_{LN} and U_{dc} are not as significant compared to variations in the relative load reduction η_e. As can be seen in Fig. 7(b), variations in droplet size after t_T = 6 mins exposed to the different excitation schemes are relatively small, with the largest difference $\Delta m_d < 5\%$, suggesting that changes to droplet size do not contribute appreciably to the increase in the relative reduction of the bacterial load (Fig. 7(a)). As reported in the earlier

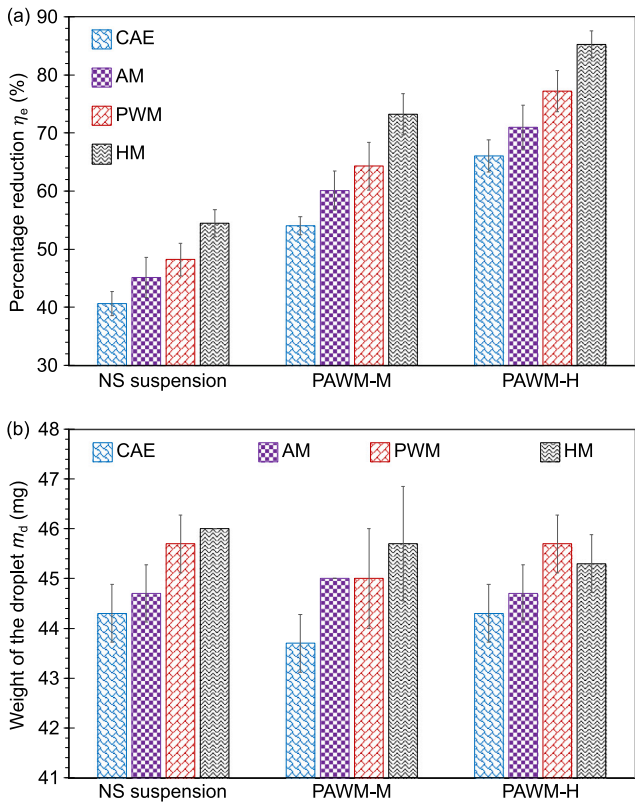

Fig. 7. (a) Relative load reduction η_e, and, (b) droplet mass m_d, for *E. coli* bacteria suspended in normal saline (NS), and two different PAW mixtures (PAWM-M and PAWM-H) following exposure to different acoustic excitation: constant-amplitude excitation (CAE), amplitude modulation (AM) with modulation frequency $f_m = 1$ kHz and modulation index $m = 0.5$; pulse-width modulation (PWM) with time ratio $R_t = 0.5$; and hybrid modulation (HM) with $f_m = 1$ kHz, $m = 0.5$ and $R_t = 0.5$. The excitation power was fixed at approximately $P_e \approx 68$ mW while the acoustic treatment duration was fixed at $t_T = 6$ mins. The standard deviation in η_e for each condition was independently calculated from triplicate experiments.

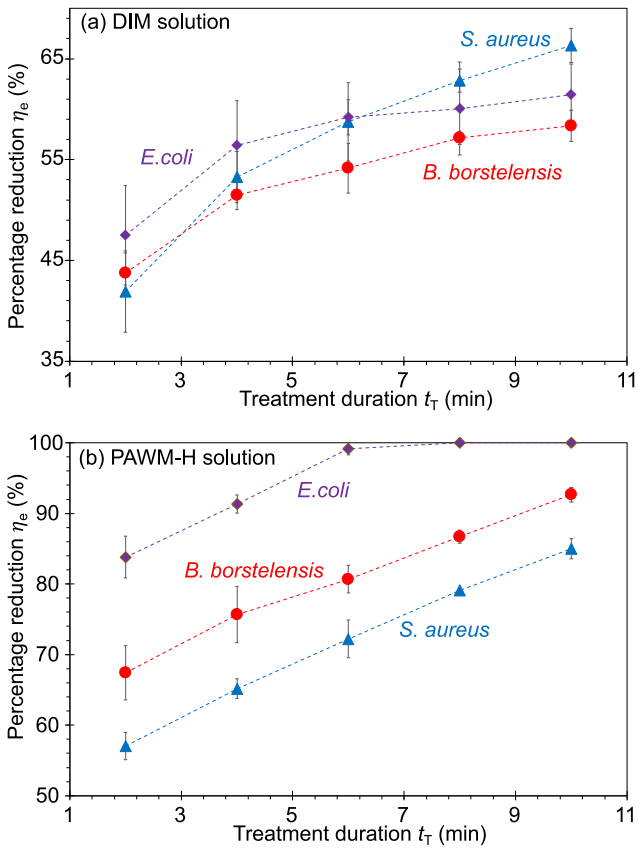

Fig. 8. Relative reduction in bacterial load η_e as a function of the SAW treatment duration ($t_T = 0$, 2, 4, 6, 8 and 10 mins) for different bacteria suspensions ((▲) *S. aureus* (gram-positive), (•) *B. bortelensis* (gram-positive) and (◆) *E. coli* (gram-negative)) at an excitation power of $P_e = 380$ mW. The bacteria were suspended in (a) diluted normal saline (DIM), and, (b) PAW mixture (PAWM-H), as defined in Table 1. Amplitude modulation with a modulation frequency $f_m = 1$ kHz and modulation index $m = 0.5$ was employed for the excitation. Trendlines (dotted lines) were added to aid visualization and the standard deviation in η_e for each condition was independently calculated from triplicate experiments.

study [64], the differences in the steady-state temperature on the surface of the LN substrate under these four excitation schemes are also relatively small (<2 °C), with the surface temperature under the hybrid modulation scheme being comparable to that for constant-amplitude excitation. Finally, by measuring the average velocities at 4 mW SAW excitation power by tracking the motion of polystyrene microparticles in the droplet under the influence of the acoustic streaming ($U_{dc} \approx 0.4 \pm 0.2$ μm/s, 0.8 ± 0.3 μm/s, 0.6 ± 0.4 μm/s and 0.9 ± 0.5 μm/s for the constant-amplitude excitation, amplitude modulation, pulse-width modulation, and hybrid modulation schemes, respectively), we observe only a modest increase in the streaming velocity with the hybrid modulation scheme that is still insufficient to drive shear-driven bacterial lysis.

3.4. Inactivation of Gram-positive bacteria with a MHz-order acoustic field and plasma-activated water

We finally demonstrate the effectiveness of the SAW platform with the modulation scheme in concert with PAW for inactivating Gram-positive bacteria such as *S. aureus* and *B. borstelensis*—which is considerably more difficult than Gram-negative bacteria as they have significantly (by roughly an order of magnitude) thicker cell walls compared to Gram-negative bacteria (approximately 10^{-8} m for Gram-positive bacteria and 10^{-9} m for Gram-negative bacteria [77]), although having similar pore sizes [78,79]. As can be seen in Fig. 8(a), we observe that the relative load reduction for *B. borstelensis* to be slightly lower than that for *E. coli* across all acoustic treatment durations when suspended in diluted saline DIM solutions. Noting that *B. borstelensis* has a similar rod-like shape to *E. coli*, but is smaller in diameter ($\phi_{B.bor.} \approx 0.2$–$0.5$ μm) and longer in length ($L_{B.bor.} \approx 2$–15 μm) [80] this suggests that the effect of the MHz-order acoustic field has a slightly stronger impact on Gram-negative (*E. coli*) bacteria due to their thinner cell wall. In contrast, *S. aureus* is round-shaped and has a diameter of approximately $\phi_{S.aures} \approx 0.5$–$1.5$ μm. Given a Young's modulus for *S. aureus* and *E. coli* of approximately 1.3 ± 0.2 MPa and 3.7 ± 0.3 MPa, respectively, we therefore expect *S. aureus* to experience larger deformations compared to *E. coli* for the same acoustic radiation pressure imposed on it. For shorter acoustic treatment durations ($t_T < 6$ mins), the relative load reduction for *S. aureus* is nevertheless lower than that for *E. coli*, again alluding that its thicker cell wall endows it with better protection. For longer acoustic treatment durations ($t_T > 6$ mins), however, we observe the relative load reduction for *S. aureus* to nevertheless be higher than that for *E. coli*, suggesting that prolonged exposure to the acoustic field leads to unavoidable damage in spite of the cell wall thickness. This is likely because the MHz-order acoustic forcing is also known to facilitate ion influx (e.g., Ca^{2+}) into the cell by permeabilizing its membrane [81–86]—with prolonged exposure, sustained high levels in intracellular ion concentrations above the basal state can lead to apoptosis if the cell is unable to remove the excess ion concentration to maintain homeostasis.

In general, the qualitative effect of the acoustic field on the Gram-negative bacteria (*E. coli*) and Gram-positive bacteria (*S. aureus* and *B. borstelensis*) appears to be similar when the bacteria suspended in

diluted normal saline DIM solution, as depicted in Fig. 8(a). At each treatment duration, the relative load reductions estimated for the three different bacteria are relatively close, with the largest difference at a given t_T value being only $\Delta\eta_e \approx 8\%$. However, a distinct difference emerges when bacteria are suspended in the PAW mixture (PAWM-H). As can be seen in Fig. 8(b), there is a notable difference in the relative load reduction among the three bacteria, with the largest difference being up to $\Delta\eta_e \approx 27\%$. The considerably stronger effect of the acoustic irradiation on Gram-negative bacteria compared to Gram-positive that is observed further affirms our aforementioned hypothesis that this is due to the thicker cell wall in the latter, which is also consistent with that reported in the literature (see, for example, Ref. [87]).

4. Conclusions

We have conducted a comprehensive investigation into the impact of MHz-order acoustic fields on bacteria suspended in various solutions, particularly at lower excitation powers compared to those used in prior studies [58,59] for which the convective acoustic streaming flow that arises is relatively weak and does not significantly contribute to shear-driven bacterial lysis. In contrast, we show in this work that it is instead the acoustic radiation force arising from the SAW excitation along the substrate which acts on the bacteria that is the dominant mechanism for their inactivation. At the highest power we examined (P_e = 380 mW), which is still an order-of-magnitude lower to preceding work, it is possible to obtain a relative reduction in bacterial load that is $\eta_e \approx 74\%$ over just t_T = 10 mins of acoustic irradiation compared to the control experiment (no acoustic treatment). We show that this efficiency for bacterial inactivation can be further improved by a further 14% adopting a hybrid modulation scheme involving a combination of amplitude and pulse-width modulation, and even further, by synergistically combining the process with plasma-activated water such that a 100% relative reduction in bacterial load can be achieved for *E. coli*. Finally, we also show that the platform is also effective in treating Gram-positive bacteria such as *B. borstelensis* and *S. aureus* (93% and 85% relative reduction, respectively), which are considerably more difficult to inactivate in general due to their thicker cell walls. Considering the portability and scalability (through massive parallelization) of the SAW devices and their associated electrical circuits, together with the ease of producing plasma-activated water with elevated reactive species concentrations that allow for effective treatment of contaminated water with substantially smaller volumes [23,88], these promising results point to the potential of this hybrid treatment platform as a promising environmentally-friendly strategy for decontaminating water supplies without undesirable by-products.

CRediT authorship contribution statement

Nicholas S.L. Chew: Data curation, Formal analysis, Methodology, Writing – original draft. **Chien W. Ooi:** Resources, Writing – review & editing. **Leslie Y. Yeo:** Resources, Writing – review & editing. **Ming K. Tan:** Conceptualization, Funding acquisition, Supervision, Writing – review & editing.

Declaration of competing interest

The authors declare that they have no known competing financial interests or personal relationships that could have appeared to influence the work reported in this paper.

Data availability

Data will be made available on request.

Acknowledgment

MKT gratefully acknowledges funding for this work from the Fundamental Research Grant Scheme, Ministry of Education, Malaysia, through Project Grant No. FRGS/1/2019/TK03/MUSM/02/1.

References

[1] W. Grabow, Waterborne diseases: Update on water quality assessment and control, Water SA 22 (2) (1996) 193–202.
[2] I. George, P. Crop, P. Servais, Use of β-d-galactosidase and β-d-glucuronidase activities for quantitative detection of total and fecal coliforms in wastewater, Can. J. Microbiol. 47 (7) (2001) 670–675.
[3] K. Rolland, N. Lambert-Zechovsky, B. Picard, E. Denamur, Shigella and enteroinvasive *Escherichia coli* strains are derived from distinct ancestral strains of *E. coli*, Microbiology 144 (9) (1998) 2667–2672.
[4] F. Qadri, A.-M. Svennerholm, A.S.G. Faruque, R.B. Sack, Enterotoxigenic *Escherichia coli* in developing countries: Epidemiology, microbiology, clinical features, treatment, and prevention, Clin. Microbiol. Rev. 18 (3) (2005) 465–483.
[5] P. Kaur, A. Chakraborti, A. Asea, et al., Enteroaggregative *Escherichia coli*: an emerging enteric food borne pathogen, Interdiscip. Perspect. Infect. Dis. 2010 (2010) 254159.
[6] Y. Nguyen, V. Sperandio, Enterohemorrhagic *E. coli* (EHEC) pathogenesis, Front. Cell. Infect. Microbiol. 2 (2012) 90.
[7] E. Näsström, N.T. Vu Thieu, S. Dongol, A. Karkey, P. Voong Vinh, T. Ha Thanh, A. Johansson, A. Arjyal, G. Thwaites, C. Dolecek, B. Basnyat, S. Baker, H. Antti, *Salmonella* Typhi and *Salmonella* Paratyphi A elaborate distinct systemic metabolite signatures during enteric fever, in: Q. Abdool Karim (Ed.), eLife 3 (2014) e03100.
[8] A.J. Silva, J.A. Benitez, Vibrio cholerae biofilms and cholera pathogenesis, PLoS Negl. Trop. Dis. 10 (2) (2016) 1–25.
[9] M.J. Messner, P. Berger, J. Javier, Total coliform and *E. coli* in public water systems using undisinfected ground water in the United States, Int. J. Hyg. Environ. Health 220 (4) (2017) 736–743.
[10] E.D. Mintz, F.M. Reiff, R.V. Tauxe, Safe water treatment and storage in the home: A practical new strategy to prevent waterborne disease, JAMA 273 (12) (1995) 948–953.
[11] M. Guo, J. Huang, H. Hu, W. Liu, J. Yang, UV inactivation and characteristics after photoreactivation of *Escherichia coli* with plasmid: Health safety concern about UV disinfection, Water Res. 46 (13) (2012) 4031–4036.
[12] W. Liu, S. Andrews, J. Bolton, K. Linden, C. Sharpless, M. Stefan, Comparison of disinfection byproduct (DBP) formation from different UV technologies at bench scale, Water Supply 2 (5–6) (2002) 515–521.
[13] S.D. Richardson, M.J. Plewa, E.D. Wagner, R. Schoeny, D.M. DeMarini, Occurrence, genotoxicity, and carcinogenicity of regulated and emerging disinfection by-products in drinking water: A review and roadmap for research, Mutat. Res.Rev. Mutat. Res. 636 (1) (2007) 178–242.
[14] A.A. Mofidi, E.A. Meyer, P.M. Wallis, C.I. Chou, B.P. Meyer, S. Ramalingam, B.M. Coffey, The effect of UV light on the inactivation of Giardia lamblia and Giardia muris cysts as determined by animal infectivity assay (P-2951-01), Water Res. 36 (8) (2002) 2098–2108.
[15] S.H. Joo, B. Tansel, Novel technologies for reverse osmosis concentrate treatment: A review, J. Environ. Manag. 150 (2015) 322–335.
[16] S. Sablani, M. Goosen, R. Al-Belushi, M. Wilf, Concentration polarization in ultrafiltration and reverse osmosis: a critical review, Desalination 141 (3) (2001) 269–289.
[17] R.E. Quick, L. Venczel, E. Mintz, L. Soleto, J. Aparicio, M. Gironaz, L. Hutwagner, K. Greene, C. Bopp, K. Maloney, et al., Diarrhoea prevention in Bolivia through point-of-use water treatment and safe storage: a promising new strategy, Epidemiol. Infect. 122 (1) (1999) 83–90.
[18] R.E. Quick, A. Kimura, A. Thevos, M. Tembo, I. Shamputa, L. Hutwagner, E. Mintz, Diarrhea prevention through household-level water disinfection and safe storage in Zambia, Am. J. Trop. Med. Hyg. 66 (5) (2002) 584–589.
[19] B.F. Arnold, J.M. Colford, Treating water with chlorine at point-of-use to improve water quality and reduce child diarrhea in developing countries: a systematic review and meta-analysis, Am. J. Trop. Med. Hyg. 76 (2) (2007) 354–364.
[20] S.D. Richardson, A. Thruston, T. Caughran, P. Chen, T. Collette, K. Schenck, B. Lykins, C. Rav-Acha, V. Glezer, Identification of new drinking water disinfection by-products from ozone, chlorine dioxide, chloramine, and chlorine, Water Air Soil Pollut. 123 (2000) 95–102.
[21] H. Komulainen, S.-L. Vaittinen, T. Vartiainen, J. Tuomisto, V.-M. Kosma, E. Kaliste-Korhonen, S. Lötjönen, R. K. Tuominen, Carcinogenicity of the drinking water mutagen 3-Chloro-4-(dichloromethyl)-5-hydroxy-2(5H)-furanone in the rat, J. Natl. Cancer Inst. 89 (12) (1997) 848–856.
[22] J. Criquet, S. Allard, Chapter five–Influence of bromide and iodide on the formation of disinfection by–products in drinking water treatment, in: T. Manasfi, J.-L. Boudenne (Eds.), Analysis and Formation of Disinfection Byproducts in Drinking Water, in: Comprehensive Analytical Chemistry, vol. 92, Elsevier, 2021, pp. 117–138.

[23] N.S.L. Chew, C.W. Ooi, L.Y. Yeo, M.K. Tan, Hybrid atmospheric pressure plasma generation and DC electrospray aerosolization of plasma-activated water for surface pathogen disinfection, Plasma Process. Polym. 20 (3) (2023) 2200128.

[24] K.S. Wong, N.S.L. Chew, M. Low, M.K. Tan, Plasma-activated water: Physicochemical properties, generation techniques, and applications, Processes 11 (7) (2023) 2213.

[25] Q. Chen, J. Li, Y. Li, A review of plasma–liquid interactions for nanomaterial synthesis, J. Phys. D: Appl. Phys. 48 (42) (2015) 424005.

[26] T. Adachi, H. Tanaka, S. Nonomura, H. Hara, S. ichi Kondo, M. Hori, Plasma-activated medium induces A549 cell injury via a spiral apoptotic cascade involving the mitochondrial–nuclear network, Free Radic. Biol. Med. 79 (2015) 28–44.

[27] C.C.W. Verlackt, W. Van Boxem, A. Bogaerts, Transport and accumulation of plasma generated species in aqueous solution, Phys. Chem. Chem. Phys. 20 (2018) 6845–6859.

[28] H. Jablonowski, A. Schmidt-Bleker, K.-D. Weltmann, T. von Woedtke, K. Wende, Non-touching plasma–liquid interaction–where is aqueous nitric oxide generated? Phys. Chem. Chem. Phys. 20 (39) (2018) 25387–25398.

[29] P.-M. Girard, A. Arbabian, M. Fleury, G. Bauville, V. Puech, M. Dutreix, J.S. Sousa, Synergistic effect of H_2O_2 and NO_2 in cell death induced by cold atmospheric He plasma, Sci. Rep. 6 (1) (2016) 29098.

[30] R. Zhou, R. Zhou, K. Prasad, Z. Fang, R. Speight, K. Bazaka, K.K. Ostrikov, Cold atmospheric plasma activated water as a prospective disinfectant: the crucial role of peroxynitrite, Green Chem. 20 (2018) 5276–5284.

[31] C. Chen, F. Li, H.-L. Chen, M.G. Kong, Aqueous reactive species induced by a PCB surface micro-discharge air plasma device: A quantitative study, J. Phys. D: Appl. Phys. 50 (44) (2017) 445208.

[32] J.S. Beckman, T.W. Beckman, J. Chen, P.A. Marshall, B.A. Freeman, Apparent hydroxyl radical production by peroxynitrite: Implications for endothelial injury from nitric oxide and superoxide, Proc. Natl. Acad. Sci. USA 87 (4) (1990) 1620–1624.

[33] V.V. Kovačević, B.P. Dojčinović, M. Jović, G.M. Roglić, B.M. Obradović, M.M. Kuraica, Measurement of reactive species generated by dielectric barrier discharge in direct contact with water in different atmospheres, J. Phys. D: Appl. Phys. 50 (15) (2017) 155205.

[34] Y.H. Kim, Y.J. Hong, K.Y. Baik, G.C. Kwon, J.J. Choi, G.S. Cho, H.S. Uhm, D.Y. Kim, E.H. Choi, Measurement of reactive hydroxyl radical species inside the biosolutions during non-thermal atmospheric pressure plasma jet bombardment onto the solution, Plasma Chem. Plasma Process. 34 (2014) 457–472.

[35] S. Ikawa, K. Kitano, S. Hamaguchi, Effects of pH on bacterial inactivation in aqueous solutions due to low-temperature atmospheric pressure plasma application, Plasma Process. Polym. 7 (1) (2010) 33–42.

[36] P. Lukes, E. Dolezalova, I. Sisrova, M. Clupek, Aqueous-phase chemistry and bactericidal effects from an air discharge plasma in contact with water: evidence for the formation of peroxynitrite through a pseudo-second-order post-discharge reaction of H2O2 and HNO2, Plasma Sources. Sci. Technol. 23 (1) (2014) 015019.

[37] X. He, J. Lin, B. He, L. Xu, J. Li, Q. Chen, G. Yue, Q. Xiong, Q.H. Liu, The formation pathways of aqueous hydrogen peroxide in a plasma-liquid system with liquid as the cathode, Plasma Sources. Sci. Technol. 27 (8) (2018) 085010.

[38] J.Y. Park, S. Park, W. Choe, H.I. Yong, C. Jo, K. Kim, Plasma-functionalized solution: A potent antimicrobial agent for biomedical applications from antibacterial therapeutics to biomaterial surface engineering, ACS Appl. Mater. Interfaces 9 (50) (2017) 43470–43477.

[39] J. Shen, Y. Tian, Y. Li, R. Ma, Q. Zhang, J. Zhang, J. Fang, Bactericidal effects against S. aureus and physicochemical properties of plasma activated water stored at different temperatures, Sci. Rep. 6 (1) (2016) 28505.

[40] R. Ma, G. Wang, Y. Tian, K. Wang, J. Zhang, J. Fang, Non-thermal plasma-activated water inactivation of food-borne pathogen on fresh produce, J. Hazard. Mater. 300 (2015) 643–651.

[41] S. Wu, Q. Zhang, R. Ma, S. Yu, K. Wang, J. Zhang, J. Fang, Reactive radical-driven bacterial inactivation by hydrogen-peroxide-enhanced plasma-activated-water, Eur. Phys. J. Spec. Top. 226 (2017) 2887–2899.

[42] Q. Zhang, R. Ma, Y. Tian, B. Su, K. Wang, S. Yu, J. Zhang, J. Fang, Sterilization efficiency of a novel electrochemical disinfectant against Staphylococcus aureus, Environ. Sci. Technol. 50 (6) (2016) 3184–3192.

[43] Y. Xu, Y. Tian, R. Ma, Q. Liu, J. Zhang, Effect of plasma activated water on the postharvest quality of button mushrooms, *Agaricus bisporus*, Food Chem. 197 (2016) 436–444.

[44] Q. Xiang, C. Kang, L. Niu, D. Zhao, K. Li, Y. Bai, Antibacterial activity and a membrane damage mechanism of plasma-activated water against pseudomonas deceptionensis CM2, LWT Food Sci. Technol. 96 (2018) 395–401.

[45] E. Dolezalova, P. Lukes, Membrane damage and active but nonculturable state in liquid cultures of *Escherichia coli* treated with an atmospheric pressure plasma jet, Bioelectrochemistry 103 (2015) 7–14, BIOELECTRICS 2013.

[46] M. Yusupov, A. Bogaerts, S. Huygh, R. Snoeckx, A.C.T. van Duin, E.C. Neyts, Plasma-induced destruction of bacterial cell wall components: A reactive molecular dynamics simulation, J. Phys. Chem. C 117 (11) (2013) 5993–5998.

[47] S.G. Joshi, M. Cooper, A. Yost, M. Paff, U.K. Ercan, G. Fridman, G. Friedman, A. Fridman, A.D. Brooks, Nonthermal dielectric-barrier discharge plasma-induced inactivation involves oxidative DNA damage and membrane lipid peroxidation in *Escherichia coli*, Antimicrob. Agents Chemother. 55 (3) (2011) 1053–1062.

[48] E.R. Kashket, Bioenergetics of lactic acid bacteria: cytoplasmic pH and osmotolerance, FEMS Microbiol. Rev. 3 (3) (1987) 233–244.

[49] Q. Zhang, Y. Liang, H. Feng, R. Ma, Y. Tian, J. Zhang, J. Fang, A study of oxidative stress induced by non-thermal plasma-activated water for bacterial damage, Appl. Phys. Lett. 102 (20) (2013) 203701.

[50] Y. Tian, R. Ma, Q. Zhang, H. Feng, Y. Liang, J. Zhang, J. Fang, Assessment of the physicochemical properties and biological effects of water activated by non-thermal plasma above and beneath the water surface, Plasma Process. Polym. 12 (5) (2015) 439–449.

[51] L. Guo, R. Xu, L. Gou, Z. Liu, Y. Zhao, D. Liu, L. Zhang, H. Chen, M.G. Kong, Mechanism of virus inactivation by cold atmospheric-pressure plasma and plasma-activated water, Appl. Environ. Microbiol. 84 (17) (2018) e00726.

[52] X. Su, Y. Tian, H. Zhou, Y. Li, Z. Zhang, B. Jiang, B. Yang, J. Zhang, J. Fang, Inactivation efficacy of nonthermal plasma-activated solutions against Newcastle disease virus, Appl. Environ. Microbiol. 84 (9) (2018) e02836.

[53] J. Julák, V. Kříha, V. Scholtz, Corona discharge: A simple method of its generation and study of its bactericidal properties, Czech. J. Phys. 56 (2006) B1333–B1338.

[54] Y. Morabit, M.I. Hasan, R.D. Whalley, E. Robert, M. Modic, J.L. Walsh, A review of the gas and liquid phase interactions in low-temperature plasma jets used for biomedical applications, Eur. Phys. J. D 75 (2021) 1–26.

[55] E. Feizollahi, N. Misra, M.S. Roopesh, Factors influencing the antimicrobial efficacy of dielectric barrier discharge (DBD) atmospheric cold plasma (ACP) in food processing applications, Crit. Rev. Food Sci. Nutr. 61 (4) (2021) 666–689.

[56] C. Lauteri, G. Ferri, A. Piccinini, L. Pennisi, A. Vergara, Ultrasound technology as inactivation method for foodborne pathogens: A review, Foods 12 (6) (2023) 1212.

[57] D.P. Chandler, J. Brown, C.J. Bruckner-Lea, L. Olson, G.J. Posakony, J.R. Stults, N.B. Valentine, L.J. Bond, Continuous spore disruption using radially focused, high-frequency ultrasound, Anal. Chem. 73 (15) (2001) 3784–3789.

[58] H. Lu, K. Mutafopulos, J.A. Heyman, P. Spink, L. Shen, C. Wang, T. Franke, D.A. Weitz, Rapid additive-free bacteria lysis using traveling surface acoustic waves in microfluidic channels, Lab Chip 19 (2019) 4064–4070.

[59] J. Reboud, Y. Bourquin, R. Wilson, G.S. Pall, M. Jiwaji, A.R. Pitt, A. Graham, A.P. Waters, J.M. Cooper, Shaping acoustic fields as a toolset for microfluidic manipulations in diagnostic technologies, Proc. Natl. Acad. Sci. USA 109 (38) (2012) 15162–15167.

[60] H. Li, J.R. Friend, L.Y. Yeo, Surface acoustic wave concentration of particle and bioparticle suspensions, Biomed. Microdevices 9 (5) (2007) 647–656.

[61] R. Shilton, M.K. Tan, L.Y. Yeo, J.R. Friend, Particle concentration and mixing in microdrops driven by focused surface acoustic waves, J. Appl. Phys. 104 (1) (2008) 014910.

[62] K.M. Ang, L.Y. Yeo, Y.M. Hung, M.K. Tan, Amplitude modulation schemes for enhancing acoustically-driven microcentrifugation and micromixing, Biomicrofluidics 10 (5) (2016) 054106.

[63] K.K. Lay, K.M. Ang, Y.M. Hung, M.K. Tan, Efficient atomization of brine at atmospheric pressure, J. Aerosol Sci. 122 (2018) 11–20.

[64] C.C. Woo, S.N. Nia, D. Gouwanda, L.Y. Yeo, M.K. Tan, Efficient modulated acoustic nebulisation for aerosol delivery and detection of plasma-activated water for surface disinfection and decontamination, Surf. Interfaces 41 (2023) 103162.

[65] L. Frenzel, Principles of Electronic Communication Systems, McGraw-Hill, 2007.

[66] K.S. Wong, W.T.H. Lim, C.W. Ooi, L.Y. Yeo, M.K. Tan, In situ generation of plasma-activated aerosols via surface acoustic wave nebulization for portable spray-based surface bacterial inactivation, Lab Chip 20 (2020) 1856–1868.

[67] N.S. Chew, K.S. Wong, W.S. Chang, C.W. Ooi, L.Y. Yeo, M.K. Tan, Nanoscale plasma-activated aerosol generation for in situ surface pathogen disinfection, Microsyst. Nanoeng. 8 (1) (2022) 41.

[68] K.M. Ang, L.Y. Yeo, Y.M. Hung, M.K. Tan, Acoustially-mediated microfluidic nanofiltration through graphene films, Nanoscale 9 (2017) 6497–6508.

[69] J.S. Chan, Y.M. Hung, M.-Z.P. Ismadi, L.Y. Yeo, M.K. Tan, Nanofiltration using graphene-epoxy filter media actuated by surface acoustic waves, Phys. Rev. A 15 (2021) 034078.

[70] S. Collignon, O. Manor, J. Friend, Improving and predicting fluid atomization via hysteresis-free thickness vibration of lithium niobate, Adv. Funct. Mater. 28 (8) (2018) 1704359.

[71] M.E. Bayer, H. Thurow, Polysaccharide capsule of *Escherichia coli*: microscope study of its size, structure, and sites of synthesis, J. Bacteriol. 130 (2) (1977) 911–936.

[72] A. Weber, M. Gibisch, D. Tyrakowski, M. Cserjan-Puschmann, J.L. Toca-Herrera, G. Striedner, Recombinant peptide production softens *Escherichia coli* cells and increases their size during C-limited fed-batch cultivation, Int. J. Mol. Sci. 24 (3) (2023) 2641.

[73] K. Yosioka, Y. Kawasima, Acoustic radiation pressure on a compressible sphere, Acoustica 5 (1955) 167–173.

[74] J.S. Chan, M. Low, P.E. Poh, L.Y. Yeo, M.K. Tan, Palm oil mill effluent processing via hybrid plasma and acoustic treatment, J. Water Process Eng. 51 (2023) 103455.

[75] J.S. Chan, P.E. Poh, M.-Z.P. Ismadi, L.Y. Yeo, M.K. Tan, Enhancing greywater treatment via MHz-order surface acoustic waves, Water Res. 169 (2020) 115187.
[76] J.S. Chan, P.E. Poh, M.-Z.P. Ismadi, L.Y. Yeo, M.K. Tan, Acoustic enhancement of aerobic greywater treatment processes, J. Water Process Eng. 44 (2021) 102321.
[77] H. Hwang, N. Paracini, J.M. Parks, J.H. Lakey, J.C. Gumbart, Distribution of mechanical stress in the *Escherichia coli* cell envelope, Biomembranes 1860 (12) (2018) 2566–2575.
[78] W. Vollmer, D. Blanot, M.A. De Pedro, Peptidoglycan structure and architecture, FEMS Microbiol. Rev. 32 (2) (2008) 149–167.
[79] B.M. Forster, H. Marquis, Protein transport across the cell wall of monoderm gram-positive bacteria, Mol. Microbiol. 84 (3) (2012) 405–413.
[80] A.B. Khalil, N. Sivakumar, M. Arslan, H. Saleem, S. Qarawi, Insights into brevibacillus borstelensis AK1 through whole genome sequencing: A thermophilic bacterium isolated from a hot spring in Saudi Arabia, BioMed Res. Int. 2018 (2018) 5862437.
[81] S. Ramesan, A.R. Rezk, C. Dekiwadia, C. Cortez-Jugo, L.Y. Yeo, Acoustically-mediated intracellular delivery, Nanoscale 10 (27) (2018) 13165–13178.
[82] S. Ramesan, A.R. Rezk, P.M. Cevaal, C. Cortez-Jugo, J. Symons, L.Y. Yeo, Acoustofection: high-frequency vibrational membrane permeabilization for intracellular siRNA delivery into nonadherent cells, ACS Appl. Bio Mater. 4 (3) (2021) 2781–2789.
[83] L.A. Ambattu, S. Ramesan, C. Dekiwadia, E. Hanssen, H. Li, L.Y. Yeo, High frequency acoustic cell stimulation promotes exosome generation regulated by a calcium-dependent mechanism, Commun. Biol. 3 (1) (2020) 553.
[84] L.A. Ambattu, A. Gelmi, L.Y. Yeo, Short-duration high frequency megaHertz-order nanomechanostimulation drives early and persistent osteogenic differentiation in mesenchymal stem cells, Small 18 (8) (2022) 2106823.
[85] L.A. Ambattu, C. Knight, K.-h. Lin, A. Gelmi, L.Y. Yeo, Calcium-dependent cAMP mediates the mechanoresponsive behaviour of endothelial cells to high-frequency nanomechanostimulation, Biomaterials 292 (2023) 121866.
[86] L.A. Ambattu, L.Y. Yeo, Sonomechanobiology: vibrational stimulation of cells and its therapeutic implications, Biophys. Rev. 4 (2023) 021301.
[87] S. Jyung, J.-W. Kang, D.-H. Kang, L. monocytogens exhibited less cell membrane damage, lipid peroxidation, and intracellular reactive oxygen species accumulation after plasma-activated water treatment compared to *E. coli* O157:H7 and *S. Typhimurium*, Food Microbiol. 108 (2022) 104098.
[88] M. Low, W.S. Sow, Y.M. Hung, M.K. Tan, Increase in leidenfrost point via plasma-activated water, Int. J. Therm. Sci. 184 (2023) 107908.